energies

Article

Heavy Multi-Articulated Vehicles with Electric and Hybrid Power Trains for Road Freight Activity: An Australian Context

Joshua Allwright [1], Akhlaqur Rahman [2,*], Marcus Coleman [3] and Ambarish Kulkarni [1]

[1] School of Engineering, Swinburne University of Technology, Hawthorn, VIC 3122, Australia
[2] School of Industrial Automation, Engineering Institute of Technology, Melbourne, VIC 3000, Australia
[3] Tiger Spider, St. Kilda, VIC 3182, Australia
* Correspondence: akhlaqur.rahman@eit.edu.au; Tel.: +61-451-321-205

Abstract: The electrification of vehicles from the automotive and public transport industries can reduce harmful emissions if implemented correctly, but there is little evidence of whether the electrification of heavy freight transportation vehicles (HFTVs), such as multi-articulated vehicles, used in the freight industry could see the same benefits. This work studied heavy multi-articulated freight vehicles and developed a comparative analysis between electric and conventional diesel power trains to reduce their total emissions. Real-world drive cycle data were obtained from a heavy multi-articulated freight vehicle operating around Melbourne, Australia, with a gross combination mass (GCM) of up to 66,000 kg. Numerical models of the case study freight vehicle were then simulated with diesel, through-the-road parallel (TTRP) hybrid and electric power trains over the five different drive cycles with fuel and energy consumption results quantified. Battery weights were added on top of the real-world operating GCMs to assure the operational payload did not have to be reduced to accommodate the addition of electric power trains. The fuel and energy consumptions were then used to estimate the real-world emissions and compared. The results showed a positive reduction in tailpipe emissions, but total greenhouse emission was worse for operation in Melbourne if batteries were charged off the grid. However, if Melbourne can move towards more renewable energy and change its emission factor for generating electricity down to 0.49 kg $CO_{2\text{-}e}$/kWh, a strong decarbonization could be possible for the Australian road freight industry and could help meet emission reduction targets set out in the 2015 Paris Agreement.

Keywords: electric vehicles; electric power trains; heavy multi-articulated vehicles; energy demand; Australian road freight industry; CO_2 emissions; fuel economy

check for updates

Citation: Allwright, J.; Rahman, A.; Coleman, M.; Kulkarni, A. Heavy Multi-Articulated Vehicles with Electric and Hybrid Power Trains for Road Freight Activity: An Australian Context. *Energies* **2022**, *15*, 6237. https://doi.org/10.3390/en15176237

Academic Editors: Akhtar Kalam, Gustavo Fimbres Weihs, Michael Negnevitsky and Georgios Konstantinou

Received: 3 August 2022
Accepted: 24 August 2022
Published: 26 August 2022

1. Introduction

Electric power trains have been heavily studied for a majority of road vehicle classes due to the body of knowledge that supports their ability to reduce emissions and local pollutants. However, the body of research around heavy freight transportation vehicles (HFTVs) with electric power trains is fairly limited. This is partly due to the diversity of HFTVs used in road freight industries (RFIs), presenting a large number of vehicles and operational cases that researchers have yet to explore. Another reason is the presumption that battery weight would become too large for suitability in HFTVs, which would result in a reduction in payload capacity [1].

Countries are looking to decarbonize their RFIs, but, so far only with higher capacity HFTVs and by adopting greener freight operational planning [2–4]. Economies around the world depend on RFIs as the most practical method to transport goods and services around the country as well as to and from a country's ports. The RFIs are one of the most energy-intensive means of transportation, leading to them being one of the highest greenhouse gas emitters in the transportation sector [5,6]. This is strongly due to industries' HFTVs running almost purely on burning fossil fuels [7,8]. Lacking a solution to reduce RFIs' greenhouse gas emissions will be a major factor in a country's ability towards minimizing its global greenhouse gas emissions to meet targets set out in the 2015 Paris Agreement [9–11]. Countries such as Australia, for example, reduce their emission impact by adopting multi-articulated vehicles over singly articulated vehicles. Increasing the load-carrying capability helps reduce the number of kilometers traveled and enhances the drag reduction benefits, similar to truck platooning [12,13]. What has not been proven or researched is if further benefits on reducing emissions could be possible with the electrification of multi-articulated vehicles.

Additionally, HFTVs tend to operate in close proximity to densely populated areas, as freight is moved to distribution centers, increasing greenhouse gases in the form of chemicals. These chemicals are carbon dioxide, carbon monoxide, nitrogen oxides (NO and NO_2, henceforth referred to as NOx), particulate matter (PM10 and PM2.5), and total volatile organic compounds [14]. The range of chemicals released is not only bad for our environment but is also bad for societal health [15,16]. Gases such as NOx cause significant health issues, sometimes leading to premature death [17]. The release of particulate matter from diesel also has a significant effect on societal health. The smaller the particulate matter is, the more harmful it is as the particles can penetrate deeper into the human lungs [18]. Therefore, methods to reduce the RFIs' dependencies on fossil fuels is highly advantageous due to the exposure our society has to HFTVs' operations, further backing the electrification of multi-articulated vehicles.

The other limitation of electrification was the increase in electricity demand that will follow. The methods used in each country to generate electricity will have a strong influence on the viability of reducing total greenhouse gas emissions and also the type of electric power train used. Studies in the U.S. showed passenger hybrids were the most energy efficient in 45 of 50 states to reduce emissions [19]. UK studies concluded that passenger vehicles with advanced combustion technologies and hybridization (parallel topology) were the best methods to reduce emissions [20]. Studies in Australia found hybrids (series and parallel topology) were the best methods to reduce emissions, which was based on the fact that no charging off the electricity grid occurred [21]. However, studies in Macau, China, from the real-world testing of electric buses around an 8.8 km route, found a 19–35% reduction in greenhouse gas emissions with charging off the grid [22]. Overall, while a cleaner power grid becomes available in different countries, the use of hybrid power trains might be the best-suited option to reduce total emissions across HFTVs' classes.

To put into context the Australian market, a total of 204.575 million tonne-kilometers (tkm) of freight movement was seen in a 12-month period between 2015 and 2016. Articulated and multi-articulated vehicles were responsible for 76.8% of the fright movement in the 12 months and used 7172 megaliters of fuel, of which 99.6% was diesel, in the process [8]. This resulted in articulated and multi-articulated vehicles being among the largest vehicle classes contributing to emission pollution. Furthermore, many areas in Melbourne have been recorded to have days exceeding the daily limit of PM10 and PM2.5 [23]. Areas of high RFI activity, near ports such as Port Melbourne, have significantly higher concentrations of particulate matter as well as other pollutions [24,25]. With the ongoing growth of RFIs, all emissions' rates will continue to climb, making research around decarbonization of RFIs particularly important for Melbourne.

With that in mind, the novelty of this paper is in addressing the decarbonization of the RFIs with the use of electric power trains on a class of HFTVs, for example, a prime mover towing two 40 ft shipping containers. To the best of our knowledge, our work is the first to study electric power trains on vehicles with a maximum weight above 40 t [1] and up to 85.5 t. Due to different laws within Australia, larger payload limits are allowed compared to the rest of the world, making it possible to offset battery weight and not reduce payload. Both pure electric and hybrid power trains were studied to analyze the decarbonization potential on freight operations. Real-world drive cycle data were recorded from multi-articulated vehicles and captured the speed and altitude changes versus time as well as operating GCMs to gain an insight into the true operational drive patterns of freight movements around Melbourne, Australia. Five drive cycles were taken as snapshots of daily operations with different GCMs over different operations. An electric power train and a battery size were then identified for all five drive cycles against operational costs and emissions' reductions. Depending on the state in Australia, there is a large difference in CO_2 emissions created per kWh, and charging in some states will lead to increased emission generation [23]. Operational costs, emissions produced from the tailpipe, and emissions produced from the electricity sectors were used as evaluation metrices in this work. The results in this paper start to fill the knowledge gap of which HFTVs benefit from electrification and breaks the presumption that large battery packs on HFTVs are not feasible. Finally, the results also presented the current status of Australia's ability to uptake HFTVs and identified key emission limits for electricity generation before claiming the required reduction in greenhouse gas emissions. These models and studies are portable to other countries with magnitude while requiring some legalities.

This paper is organized as follows. In Section 2, the background of the selected region for the case study is discussed. In Section 3, the case study vehicle is identified and we present an analysis of real-world drive cycle data. In Section 4, we present the modeling of the HFVTVs after simulations of power train components were envisaged. In Section 5, the competitive results are presented and analyzed. Finally, conclusions and recommendations based on the role of HFTVs and decarburizations are presented in Section 6.

2. Case Study Vehicle: Heavy Multi-Articulated Vehicle

Australia operates some of the largest and heaviest articulated and multi-articulated vehicles in the world. Under the performance-based scheme (PBS), a class of high-productivity freight vehicles (HPFVs) emerged; they operate at higher mass and length limits than standard global configuration vehicles [26]. HPFVs gained their name, 'high productivity', because they use less fuel and emit fewer emissions per tkm traveled on average, making HPFVs a desirable alternative to standard articulated vehicle configurations. Articulated vehicles have the highest fuel consumption, at an average 56.3 L or greater per 100 km. In this paper, a 30 m long multi-articulated vehicle was selected as the case study vehicle, as shown in Figure 1. The multi-articulated vehicle was selected because it is one of the growing vehicle combinations seen in Australia [27]; the case study area selected was Port Melbourne due to the high volume of freight vehicle activity and because it also has the state's highest road freight use [8].

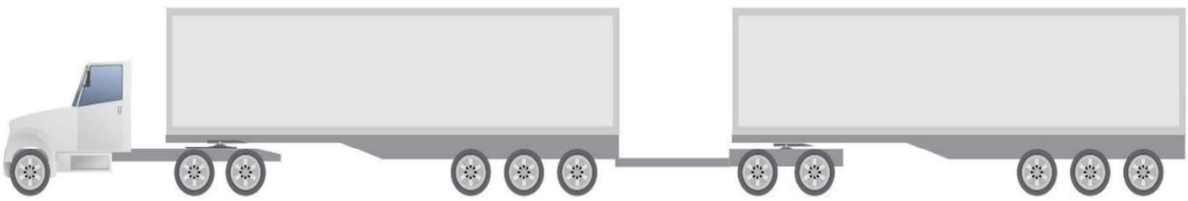

Figure 1. A 30 m, 11-axle multi-articulated vehicle.

A multi-articulated vehicle can operate up to 85,000 kg on selected routes and 68,500 kg on less restricted routes around Melbourne, which leaves potential spare weight for electric power trains, given the freight operations are volumetrically limited and not gravimetrically limited.

3. Modeling Energy Demands

In order to evaluate if electric power trains could be the path to reduce RFIs' dependencies on fossil fuels, modeling RFIs' vehicles' energy demands will allow the calculation of potential emissions saved from different power trains. A life-cycle assessments' approach is a commonly used method that starts at the raw production costs of different power train types and calculates all the emissions generated through the life cycle until the end of use [6,28–31]. However, there are limitations. A paper on Class 8 heavy vehicles in the U.S. with electric power trains can be taken as an example [32]. Through a life-cycle assessment, battery electric trucks showed improved life-cycle costs and reduced emissions based on the statistics of operational driving patterns. As emissions and economic competitiveness of different power trains are significantly linked to driving patterns [33], life-cycle assessments can incorrectly model these details when looking at new or different vehicle fleets. The acceleration and deceleration demands combined with different vehicle masses will have a strong effect on power demands [20] as well as driving distances, which all have a strong influence on the total energy required [34]. Furthermore, both NOx and particulate matter emissions exhibit significant correlations with the change in vehicle speed, acceleration, and power demand [35], making it vital to have this level of detail in the analysis while looking at RFIs' operations. Therefore, drive cycle data were collected from two multi-articulated vehicles operating around Melbourne with different GCMs used to calculate the energy demands from the new fleet.

Drive Cycles

Five real-world drive cycles are shown below in Figures 2–6 with GCMs at 43,000 kg, 50,000 kg, 55,000 kg, 61,000 kg, and 66,000 kg, respectively, taken from a selection of over 600 drive cycles recorded. Each drive cycle was selected to cover the spread of the GCM seen, which was beyond the current literature. A summary of drive cycle details are shown in Table 1.

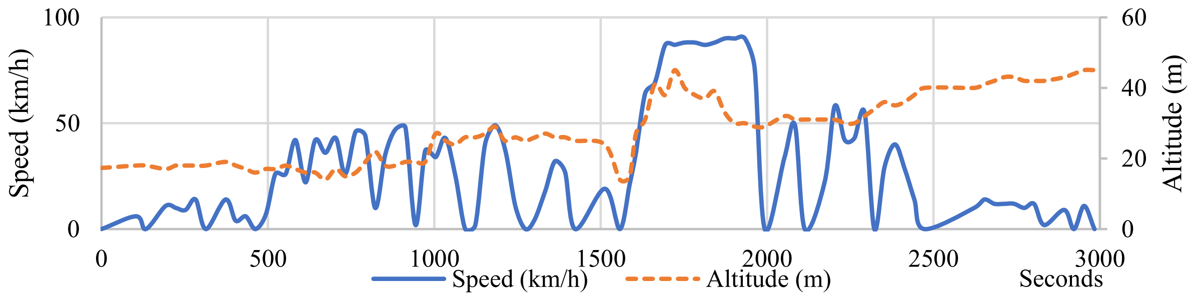

Figure 2. Drive cycle 1: GCM of 43,000 kg.

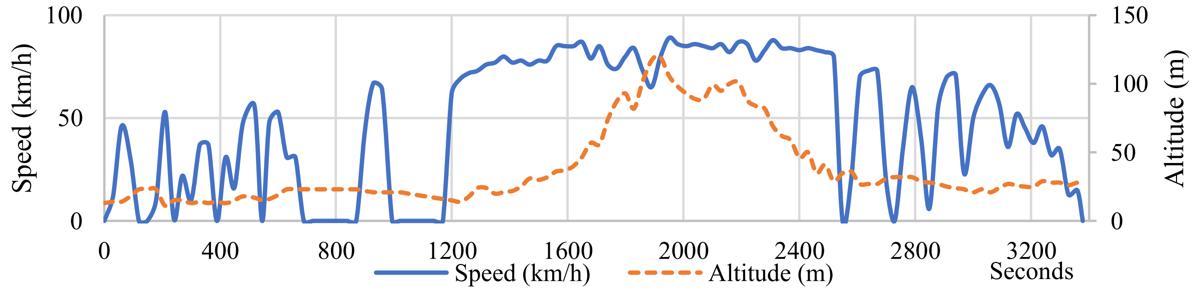

Figure 3. Drive cycle 2: GCM of 50,000 kg.

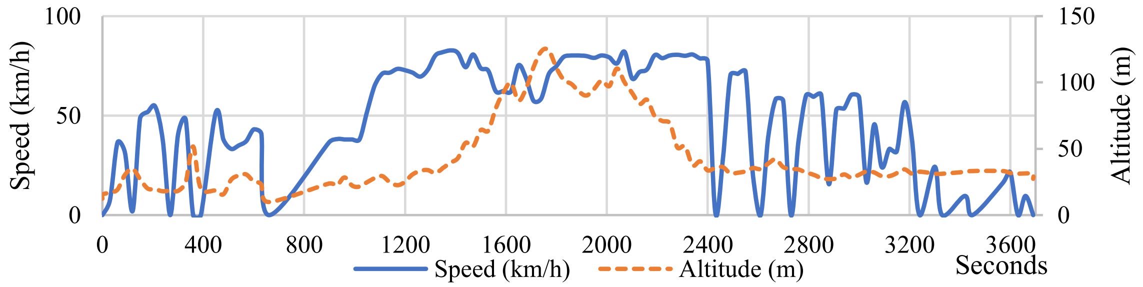

Figure 4. Drive cycle 3: GCM of 55,000 kg.

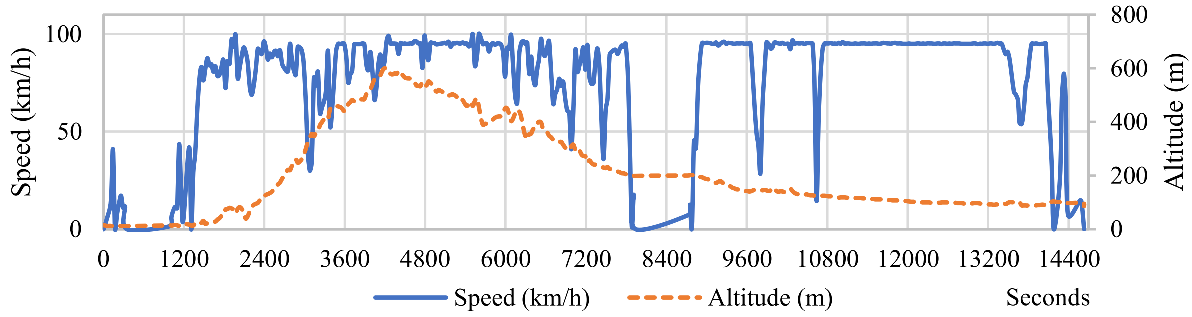

Figure 5. Drive cycle 4: GCM of 61,000 kg.

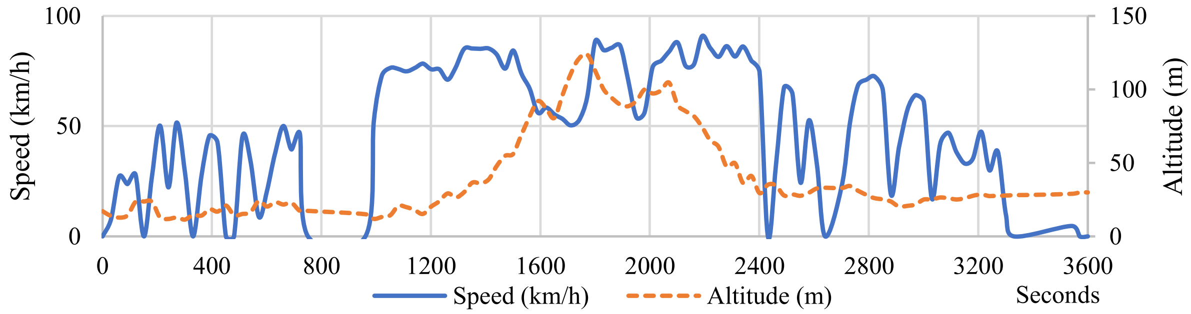

Figure 6. Drive cycle 5: GCM of 66,000 kg.

Table 1. Drive cycle summary.

Drive Cycle	GCM (kg)	Trip Length (km)	Driving Time (minutes)	Average Acc. (m/s^2)	Average Dec. (m/s^2)
1	43,000	21.7	50	0.08	0.11
2	50,000	46.2	56	0.12	0.14
3	55,000	47.0	62	0.09	0.14
4	61,000	294.7	244	0.06	0.08
5	66,000	45.6	56	0.09	0.11

4. Vehicle and Power Train Modeling

Three different power train models were created for the evaluation of the multi-articulated vehicle through means of numerical simulations, which were built in Matlab/Simulink™ (Swinburne Uni, Australia). The selected power trains were conventional diesel, through-the-road parallel (TTRP) hybrid and electric. A conventional diesel power train was used for baseline comparisons, taking the fuel burned during drive cycles and setting the comparison metric of operational costs and emissions produced. A TTRP hybrid was selected as the architecture to allow the electric power train to be installed on the trailer without the need for large modifications of the towing prime mover and, more importantly, to disconnect the coupling of the engine and motor revolutions per minute (RPM), which allowed a simplification for operating each power train in its optimal efficiency zones. Refer to Figure 7 for TTRP hybrid architecture. Battery sizes on the TTRP hybrid power train were incrementally increased until the drive cycles could be completed on electric power only or road weight limits were reached.

4.1. Vehicle Modeling

To calculate the power (P) required through the numerical simulations over different drive cycles, the standard vehicle power equations were used, with values depicted in Table 2. The vehicle was treated as a glider mass. The equation for vehicle power used is as follows [36].

$$P = F_t \cdot V_{veh} = M_{GCM} \cdot g \cdot V_{veh} \cdot (f_R + \tan\theta) + \frac{1}{2} \cdot \rho_{air} \cdot C_{drag} \cdot A \cdot {V_{veh}}^3 + M_{GCM} \cdot \frac{dV_{veh}(t)}{d(t)} \cdot V_{veh} \quad (1)$$

where F_t is the resultant force on the glider mass, V_{veh} is vehicle speed, the M_{GCM} is the vehicle mass, g is the (acceleration) due to gravity, f_R is the rolling resistance force, θ the road grade angle, p_{air} is the air density, C_{drag} is the coefficient of drag, and A is the frontal surface area in the direction of the drag. Transmission details and efficiency, shown in Table 3, were corrected to match a fuel consumption average of 1.81 km/L found in a real operation.

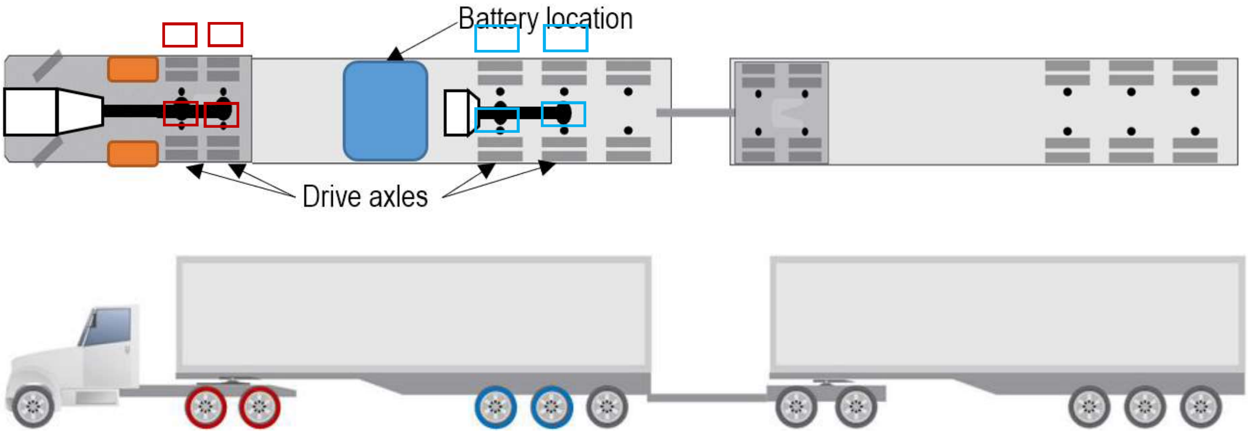

Figure 7. Top and front views of a TTRP hybrid multi-articulated vehicle: Red wheels: traction from diesel engine; blue wheels: traction from electric motor.

Table 2. Multi-articulated vehicle specifications.

Loaded tire radius (m)	0.492
Rolling resistance coefficient	0.0065
Air density (kg/m^3)	1.2
Combination C_{drag} A (m^2)	9.67 [37]

Table 3. Transmission details.

Transmission	Mack AT262D 12 Speed
Transmission efficiency (%)	95.0
Final drive ratio for combustion/electric	3.42:1
Final drive ratio for TTRP hybrid	4.5:1
Final drive efficiency (%)	98.0

4.2. Engine and Motor Modeling

A Mack MP8 500 diesel engine and a TM4 SUMO HD HV3500-9P-L-01 electric motor were selected because both had approximately the same power output. Empirical data from components were used for power and torque maps, as depicted in Figure 8 for the selected engine and motors. For the engine, a 600 hp, 15 L engine efficiency map was sourced from the EPA's Greenhouse Gas Emissions Model (GEM) for medium- and heavy-duty vehicle compliance (Phase 2 GEM simulation model data). The operational zone was limited to the Mack MP8 500 engine curves. For the TM4 motor, empirical test data of motor and controller efficiency maps were provided under a non-disclosure agreement (NDA).

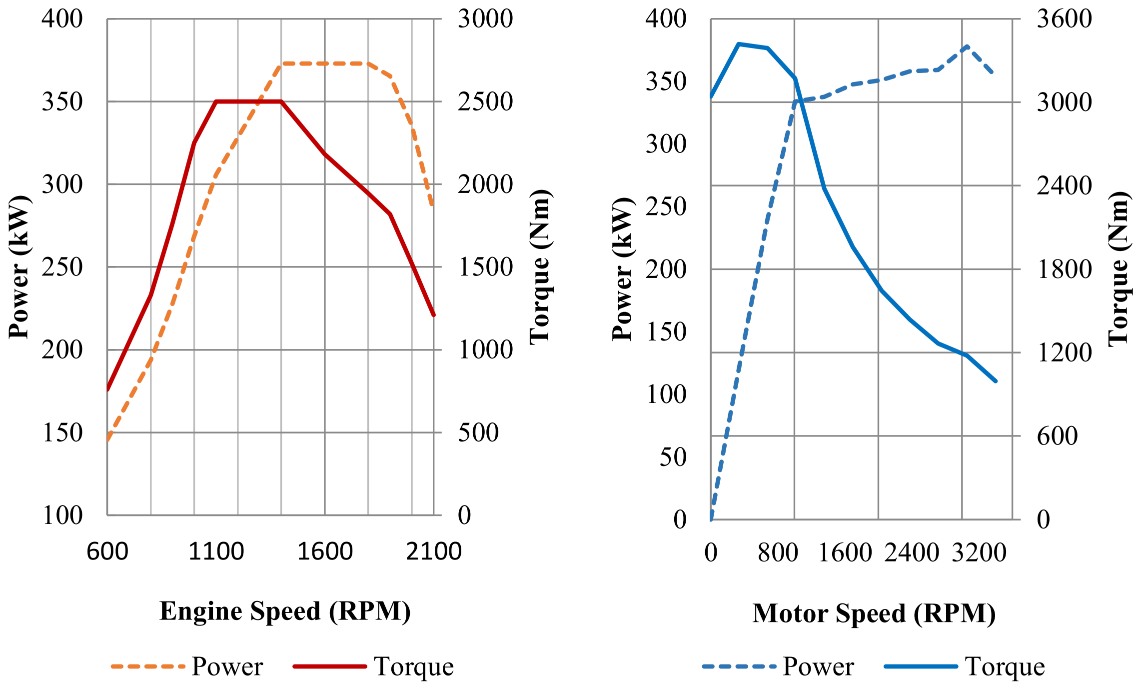

Figure 8. Right: diesel engine map; left: electric motor map.

4.3. Transmission Modeling

In order to mimic real work energy consumption from a numerical simulation, engine and motor models were paired with a transmission and/or differential for gear changes, which changed the operational points on the engine or motor during the drive cycle. The identification of these operational points on the engine or motor were cross-referenced with efficiency maps to identify fuel consumption rates or operational efficiency. Therefore, a custom gear changing logic was created to simulate transmissions changing gears automatically throughout the simulation using fundamentals of transmission operations [36]. Two main equations were used for the logic to find the minimum and maximum vehicle speeds in all possible gears. These equations were:

$$Vehicle\ Speed\ for\ Gear\ bottom\ limit = \frac{Min\ RPM \cdot \pi \cdot Tire_{Dyn} \cdot 0.12}{R_{final\ drive} \cdot R_i} \tag{2}$$

$$Vehicle\ Speed\ for\ Gear\ upper\ limit = \frac{Max\ RPM \cdot \pi \cdot Tire_{Dyn} \cdot 0.12}{R_{final\ drive} \cdot R_i} \tag{3}$$

where *Min RPM* and *Max RPM* are the lowest and highest rpm allowed from the engine or motor, respectively, $Tire_{Dyn}$ is the loaded tire radius, $R_{final\ drive}$ is the final drive ratio, and R_i is the gear ratio. Solving these two equations allows an understanding of combinations of gears versus different speeds. During the simulation time steps, the current engine or motor rpm was checked against two points: (1) a combination of possible gears and (2) the gear that operates close to the high-efficiency zone of the engine or motor. Using this logic, the need for a fixed shifting schedule map was removed to gain the flexibility of swapping different transmissions, final drive ratio, engines, or motors while still evaluating the power train at its most efficient operation points where possible. Details of the transmission used in this research are depicted in Table 3. For the TTRP hybrid model, a fixed transmission/final drive ratio was used. An electric power train was paired with the same transmission as the diesel power train.

4.4. Battery Modeling

For the use of TTRP hybrid and electric power trains, a scalable prismatic battery (e.g., lithium ion) model was built from fundaments using Ohm's, Joule's, and Kirchhoff's voltage laws with the method of Coulomb counting for updating the state of charge (SoC). Joule's law, also known as Joule's heating, was used to account for efficiency losses in the battery, taking the heat generated and adding it back onto the power demands as energy was used in removing battery heat.

The model started by selecting a rough battery size (kWh), operational voltage (V_{sys}), and cell type. A prismatic cell was used in this research with the values of 9.2 kg per kWh (which includes cooling, BMS, and packing weight) [38] and a packaging volume of 0.008 m^3/kWh [39]. The number of cells in series and parallel were then calculated with values, as shown in Table 4 and Equations (4)–(6) below.

$$C_s = Round\ down(\frac{V_{sys}}{V_{c-nomial}}) \tag{4}$$

$$C_p = Round\ down(\frac{kWh \cdot 1000}{C_s \cdot V_{C-max} \cdot C_{cap}}) \tag{5}$$

$$Cap_{max} = C_p \cdot C_{Cap} \tag{6}$$

where C_s is the number of cells in series, $V_{c-nomial}$ is the cell nominal voltage, C_p is the number of cells in parallel, C_{cap} is the cell capacity, and Cap_{max} is the actual possible battery capacity at 100% SoC.

Table 4. Cell details.

Cell Type	Prismatic Cells
Max/Nominal/Min Voltage (V)	3.85/3.22/2.41
Cell Capacity (Ah)	10
Internal Resistance (mΩ)	1.3
Discharge C Rating (Peak)	10
Charge C Rating (Peak)	4

With values set for the scalable battery model, Ohm's, Joule's, and Kirchhoff's voltage laws were combined, as illustrated in Figure 9a, which started with the power demanded at a given time step, in which positive power demand in Watts is drained from the battery and negative power demand in Watts is reclaimed from regenerative braking.

Where P_{Batt} is the power demand, V_{Term} is the battery terminal system voltage, I_{D1} is the current passed in or out of the battery, R_i is the cells' internal resistance, Q_{loss} is the heat generated by one cell, $\eta_{cooling}$ is the efficiency of the cooling system to remove heat from the battery, which was taken at 40% efficiency, I_{D2} is the current required to remove the heat from the battery pack, and I_T is the total current used in the battery at the given time step (t_s), which is used to calculate the amp hours, Ah, used for that time step.

The Ah is collected as a running sum and subtracted from $Cap_{max,}$ which is calculated using Equation (6) to find the current battery capacity, Cap_{spc}. The Cap_{soc} was then compared against Cap_{max} to find the current SoC.

To assure SoC is updated as power flows into and out of the battery model, Kirchhoff's voltage law was used to update the battery's V_{Term}; SoC can be correlated to the cell voltage (refer to curve depicted in Figure 9b) using Kirchhoff's voltage law. At each time step of the numerical simulation, the cell voltage, V_c, obtained from cell voltage versus SoC curve were multiplied by the number of cells in series, C_s, to find the open circuit voltage, V_{oc}. With V_{oc}, the total voltage drop across cell resistors $(R_i \cdot C_s \cdot I_T)$, the updated V_{Term}, was calculated and sent back to the model start phase for the next time step simulations.

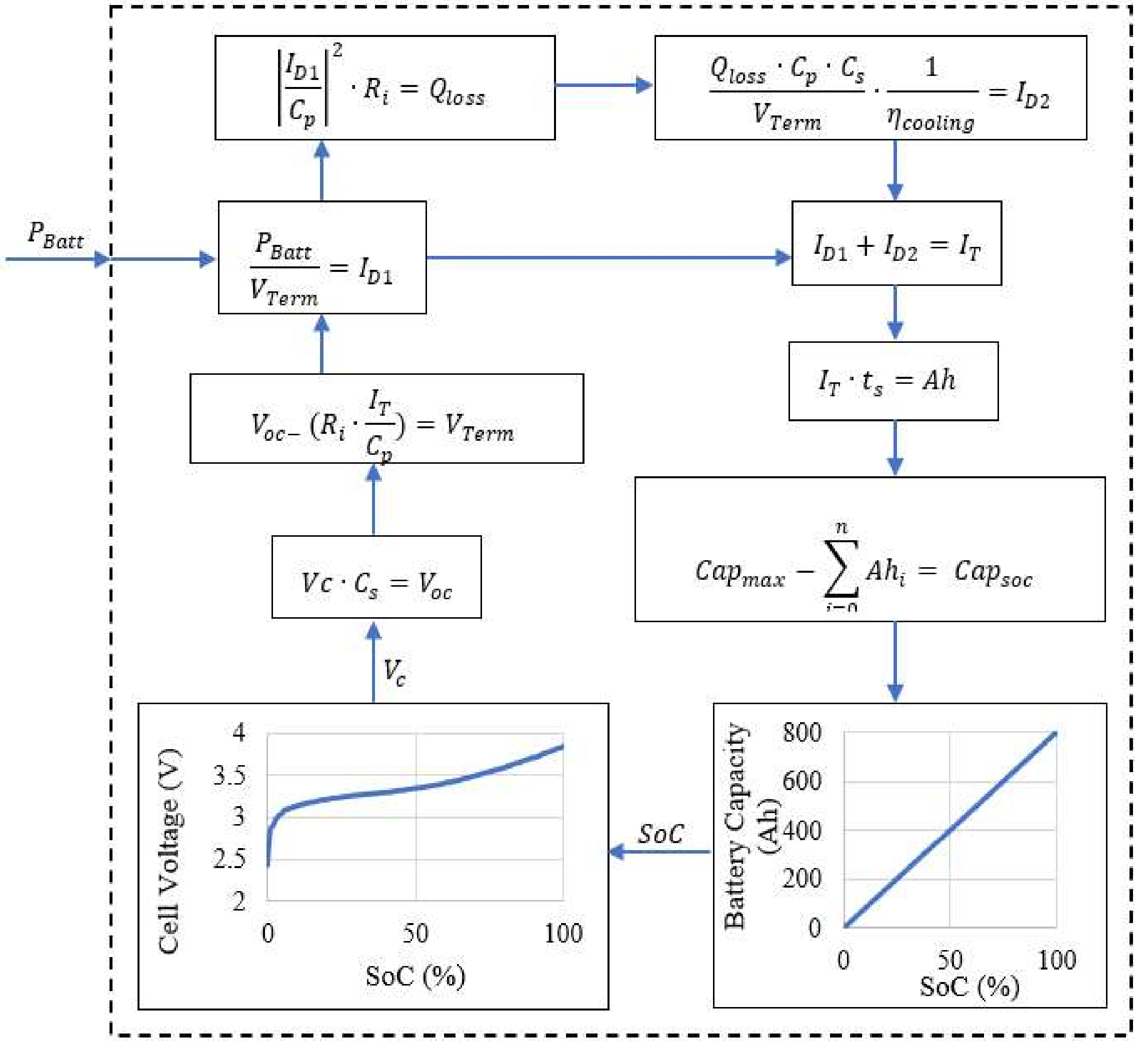

(a)

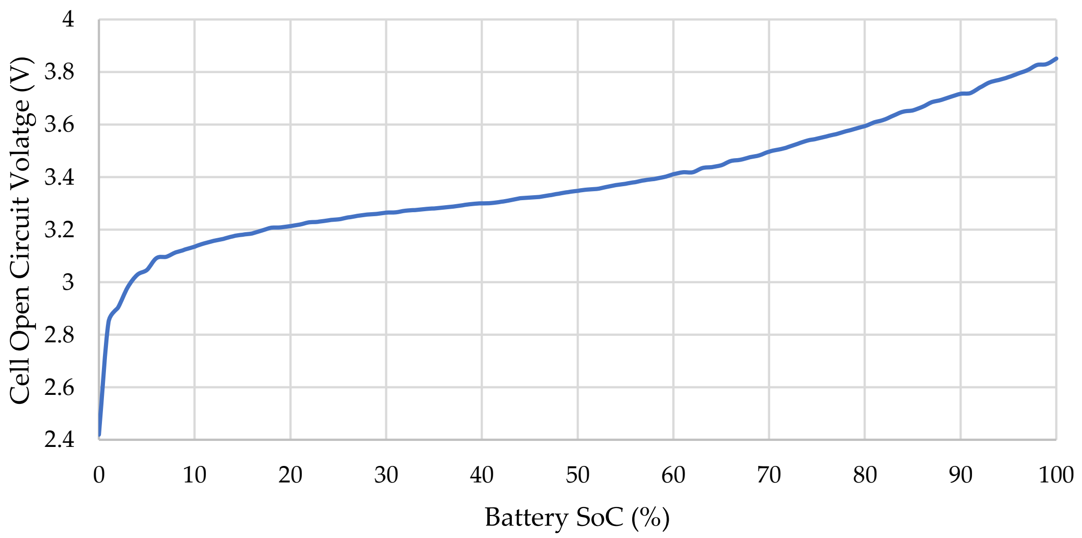

(b)

Figure 9. (**a**) Scalable prismatic battery model with cooling system; (**b**) cell OCV curve used in simulations.

Limitations of the scalable battery model were the cell resistance changes with battery temperatures [40]; however, this was addressed by assuming the worst case for initial resistance throughout all operational SoCs and battery temperatures. Battery degradation should also be included when considering the life cycle costs [41] but was ruled outside the scope of this research.

4.5. TTRP Hybrid Power-Split Modeling

There are plenty of proposed models and research methods to share energy demand between different power trains [42–46]. In this work, the selection of the amount of power sent to the diesel power train and to the electric power train for the TTRP hybrid was based around two rules. (1) Low speeds, which are common in port operations, lead to lower exhaust temperatures affecting the selective catalytic reduction systems' efficiency [47]; therefore, a low speed driving power was supplied through the electric power train to not only save fuel but to reduce low-powered engine operations. (2) Keeping the diesel engine away from the high-power range and high exhaust temperatures helped reduced emissions. High exhaust temperatures helped break down the particulate matter through burning them off; however, particulate matter became smaller in this process and, once again, affected the selective catalytic reduction system's efficiency [48].

Therefore, in the power-split model, a fixed zone of operation around the most operationally efficient point of the diesel engine was the ideal operation zone. The center of the ideal operation point is referred to as 'power mid-point'. From the power mid-point, a defined amount of power, referred to as 'power radius', was specified; this indicated the operational zone in which the engine can operate. In this research, the power mid-point was set at 151 kW and a power radius of 50 kW, which led to the power output range of the engine being between 199 kW and 301 kW. However, depending on the battery's capacity, the power radius was changed to seek the optimal power split. An example is depicted in Figure 10. To save the most fuel with any battery capacity, the power radius needed to be adjusted to allow the end of the trip SoC to be at a full discharge state (set at 30%).

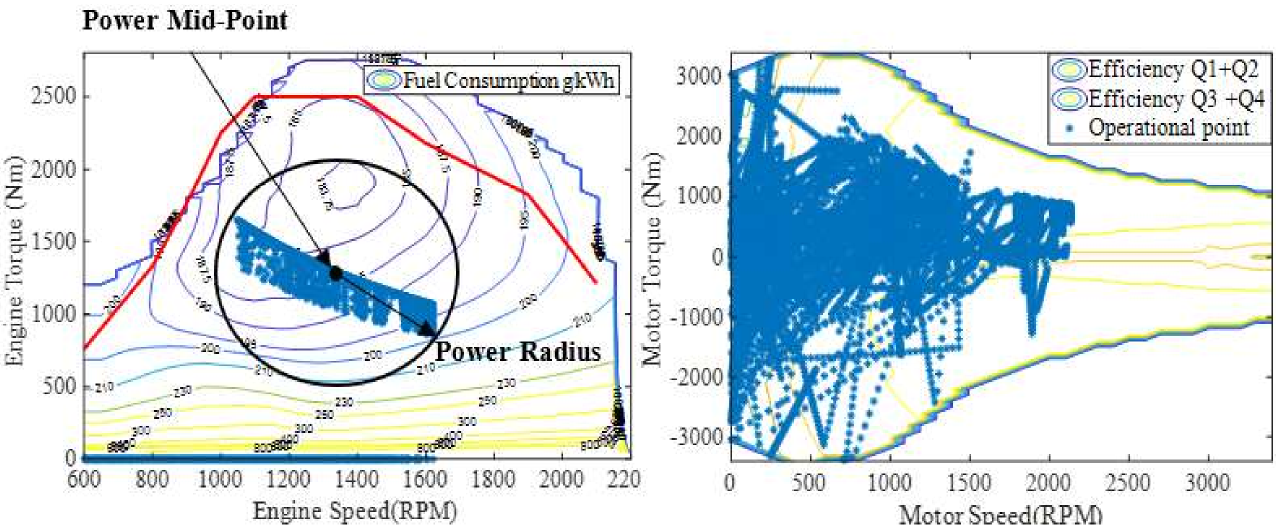

Figure 10. (**Left**): 600 hp, 15 L GEM fuel map restricted to MP8 operating range and power radius. (**Right**): TM4 motor efficiency map.

For example, when the battery's SoC at the end of the trip ended at 40%, the power radius was decreased to allow more power from the electric motor, hence minimizing fuel consumption. When the battery's SoC went to 30% before the trip, the power radius was increased to reduce the electric motor power; this stopped the engine from operating in all zones as well as towing extra weight with reduced benefits.

5. Results and Discussion

All drive cycles were simulated over the different power trains and different battery sizes. During simulations, two rules were followed. (1) Fast charging was the only method to charge the battery and, therefore, all trips started with the battery's SoC at 80%. (2) The SoC of the battery was not allowed to drop below 30% to permit fast charging to start at the end of operation, as shown in Figure 11.

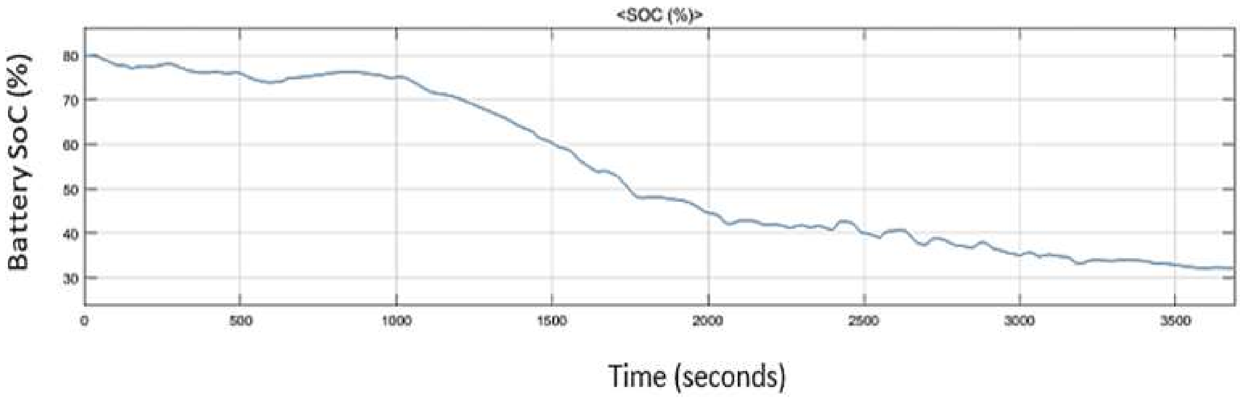

Figure 11. SoC discharge between 80% SoC to 30% SoC over drive cycle 3.

Each vehicle was simulated at its operational GCM over the drive cycles to find its fuel consumption for the trip, economy, and equivalent tail pipe GHG emissions ($CO_{2\text{-}e}$), as shown in Table 5. From the baseline, the TTRP hybrid power trains were simulated, and the weight of the electric power train and battery pack sizes were added to the GCM. In order to maintain the operational conditions of the multi-articulated vehicle, the GCM limits were set at 68,500 kg, which was a maximum of 2550 kg added by the electric power train. The electric motor and controller were set at a weight of 376 kg, which left 2174 kg for the battery weight. At 9.2 kg per kWh, the max battery size allowed on all power trains was set at 236 kWh. The TTRP hybrid started with a 50 kWh battery and was scaled in size until pure electric power was attained or a battery size of 236 kWh was reached.

Table 5. Baseline fuel and emission results.

Drive Cycle	Fuel Burned (L)	km/L	Trip Tailpipe GHG Emissions (kg $CO_{2\text{-}e}$)
1	12.02	1.81	32.7
2	23.45	1.97	63.8
3	24.67	1.90	67.1
4	165.7	1.78	450.7
5	26.86	1.70	73.1

5.1. Financial Analysis

The results of each drive cycle are shown below in Tables 6–10. At first glance, large fuel savings were achieved with the addition of a TTRP Hybrid power train or swapping to an electric power train, even with the increase in GCM. The electric power train operated in the inefficiency zones of the diesel power train, saving fuel normally burned in high-load operations such as accelerating, as shown in Figures 12 and 13. The higher GCMs (e.g., above 66,000 GCM) were not simulated as pure electric power trains to stay within the operational weight limits of 68,500 kg, resulting in only the TTRP hybrid being simulated for these weight classes.

Table 6. Drive cycle 1 results.

Power Train	GCM (kg)	Battery Size (kWh)	Fuel Burned (L)	km/L	kWh Used	km/kwh	Fuel Saved (%)
Diesel	43,000	0	12.02	1.81	0.00	0.00	0.00
TTRP Hybrid	43,574	21	7.23	3.01	8.87	2.45	39.9
TTRP Hybrid	43,837	50	4.19	5.19	20.47	1.06	65.2
TTRP Hybrid	44,035	71	2.33	9.32	28.72	0.76	80.6
Electric	44,365	100	0.00	0.00	41.43	0.52	100.0

Table 7. Drive cycle 2 results.

Power Train	GCM (kg)	Battery Size (kWh)	Fuel Burned (L)	km/L	kWh Used	km/kwh	Fuel Saved (%)
Diesel	50,000	0	23.45	1.97	0.00	0.00	0.0
TTRP Hybrid	50,837	50	14.08	3.28	20.12	2.30	40.0
TTRP Hybrid	51,299	100	9.25	5.00	38.76	1.19	60.5
TTRP Hybrid	51,760	150	6.85	6.75	60.29	0.77	70.8
Electric	52,221	200	0.00	0.00	83.46	0.55	100.0

Table 8. Drive cycle 3 results.

Power Train	GCM (kg)	Battery Size (kWh)	Fuel Burned (L)	km/L	kWh Used	km/kwh	Fuel Saved (%)
Diesel	55,000	0	24.67	1.90	0.00	0.00	0.0
TTRP Hybrid	55,837	50	15.55	3.02	20.90	2.25	37.0
TTRP Hybrid	56,298	100	10.51	4.47	40.36	1.16	57.4
TTRP Hybrid	56,760	150	8.28	5.67	60.96	0.77	66.4
TTRP Hybrid	57,221	200	6.11	7.69	80.83	0.58	75.2
Electric	57,484	229	0.00	0.00	94.79	0.50	100.0

Table 9. Drive cycle 4 results.

Power Train	GCM (kg)	Battery Size (kWh)	Fuel Burned (L)	km/L	kWh Used	km/kwh	Fuel Saved (%)
Diesel	61,000	0	165.70	1.78	0.00	0.00	0.0
TTRP Hybrid	61,837	50	152.10	1.94	21.44	13.75	8.2
TTRP Hybrid	62,298	100	148.30	1.99	39.40	7.48	10.5
TTRP Hybrid	62,759	150	144.80	2.04	59.72	4.93	12.6
TTRP Hybrid	63,221	200	140.70	2.09	81.27	3.63	15.1
TTRP Hybrid	63,550	236	136.20	2.16	98.06	3.01	17.8

Table 10. Drive cycle 5 results.

Power Train	GCM (kg)	Battery Size (kWh)	Fuel Burned (L)	km/L	kWh Used	km/kwh	Fuel Saved (%)
Diesel	66,000	0	26.86	1.70	0.00	0.00	0.0
TTRP Hybrid	66,837	50	18.87	2.42	20.52	2.22	29.7
TTRP Hybrid	67,298	100	13.60	3.36	41.35	1.10	49.4
TTRP Hybrid	67,759	150	10.24	4.46	62.15	0.73	61.9
TTRP Hybrid	68,221	200	7.80	5.85	80.91	0.56	71.0
TTRP Hybrid	68,500	236	5.53	8.25	98.24	0.46	79.4

To gain a net position of the operational savings during a trip, the cost to replace the energy used and fuel burned was considered. To understand the feasibility of operating fleets, the current costs of fuel at $1.40 per liter of diesel and $0.23 per kWh for electricity were applied to the values of used energy (fuel and electricity) (from Tables 6–10), which resulted in the findings shown in Figure 14.

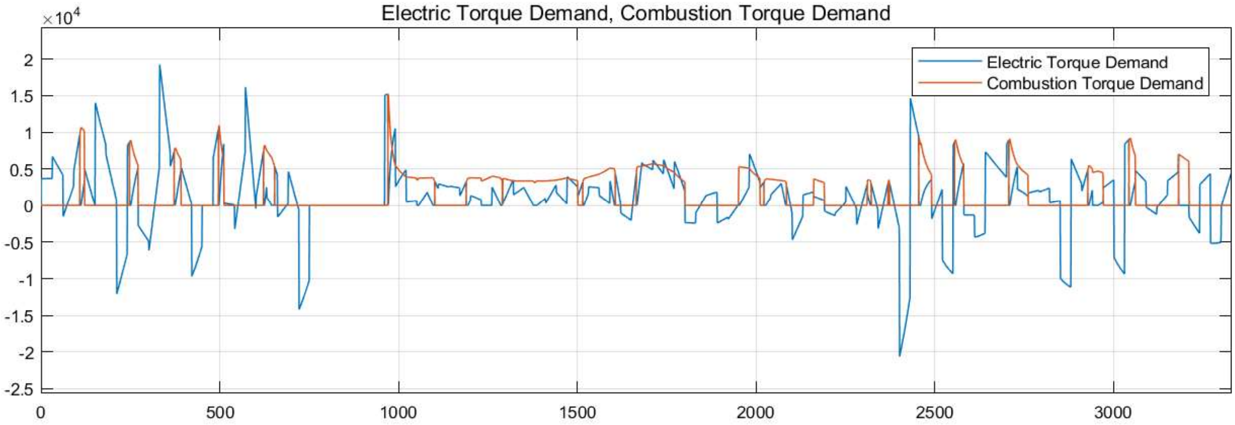

Figure 12. Power split on TTRP hybrid: torque demand from electric motor and torque demand from diesel engine.

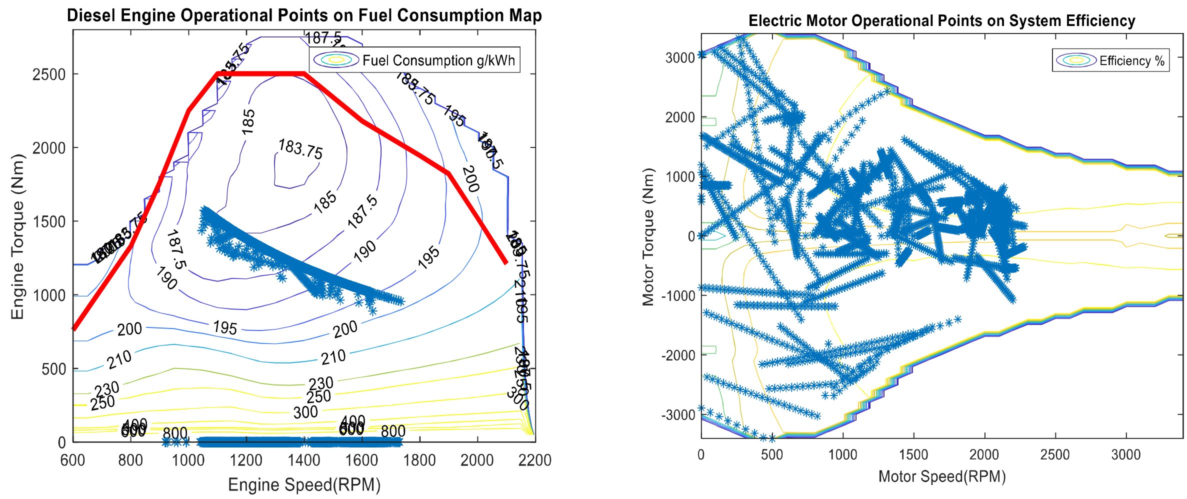

Figure 13. Operational points on diesel engine and electric motor during drive cycle. * Operational point.

Figure 14. Percentage saved over operating with diesel power train alone.

For the current fuel and electricity prices as well as the overall operational strategy proposed for fast charging at each trip's destination, a battery size of around 100 kWh was the best return for all drive cycles compared. Due to the trip length and GCM, the amount of energy required influenced the power split between the diesel engine and electric motor operational points. To achieve fuel consumption reduction with larger battery sizes, the best power mid-point of the diesel engine was not able to be maintained due to power being restricted, which lowered the amount of power coming out and pushed the operational zones into less efficient zones of the engine, as shown in Figure 15.

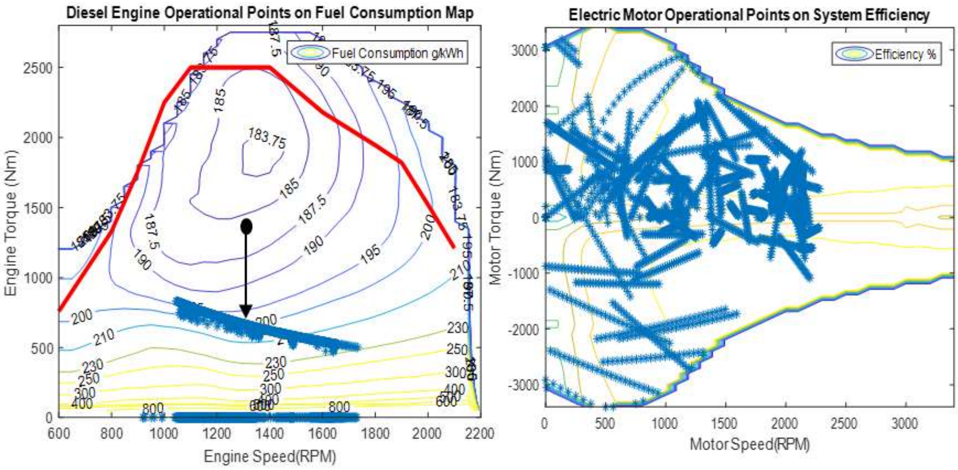

Figure 15. Engine power mid-point reduced and motor operational points from drive cycle 5 with TTRP hybrid power train and 236 kWh battery. * Operational point.

Pairing the right sized engine for the TTRP hybrid power train application with the right catalytic reduction systems is an important recommendation to consider when selecting the battery sizes. Overall, less fuel was burned with all electric power train types, resulting in less tailpipe emissions, but the local creation of particulate matter around the fleet operation remained the same if catalytic reduction systems were not able to work always in their most efficient zone.

Furthermore, with current battery weights and prices applied, the decision to use either TTRP hybrid power trains or just electric power trains will be determined based on the turning point, as shown below in Figure 16. For the TTRP hybrid, a battery size of 100 kWh should be selected for the best savings performance. Increasing the battery size on the TTPR hybrid past 100 kWh started to reduce the operational cost benefits; it is recommended to swap to a pure electric power train for a further reduction in operational savings.

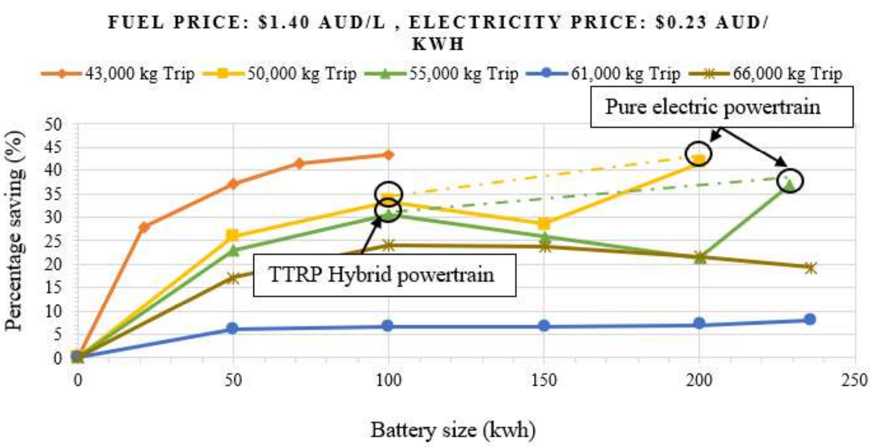

Figure 16. Strategy for electric power train selected for continuous upwards trend of operational cost savings.

5.2. Emission Analysis

Based on fuel consumption and energy used, emission factors were used to estimate the GHG emissions released during operations. The Australian government publishes yearly reports of current emission factors, and the August 2021 National Greenhouse Accounts Factors report was used in this analysis [23]. From the report, each state or territory in Australia has an electricity consumption emission factor calculated based on the methods used to generate electricity. The values assigned to each state or territory can be found in Table 11.

Table 11. Emission factors for consumption of purchased electricity or loss of electricity from the grid [23].

State or Territory	Emission Factor Kg $CO_{2\text{-}e}$/kWh
New South Wales and Australian Capital Territory	0.79
Victoria	0.96
Queensland	0.80
South Australia	0.35
South West Interconnected System (SWIS) in Western Australia	0.68
North West Interconnected System (NWIS) in Western Australia	0.58
Darwin-Katherine Interconnected System (DKIS) in the Northern Territory	0.54
Tasmania	0.16
Northern Territory	0.57

The worst-performing state in Australia was Victoria, the state of the real-world case study vehicle used in this research. Therefore, an emission factor of 0.96 kg $CO_{2\text{-}e}$/kWh was used for the emission costing the batteries' energy consumptions. From this report, emission factors for burning diesel fuel in transportation operations were also used and are shown in Table 12. The values in Table 12 and 0.95 kg $CO_{2\text{-}e}$/kWh were used to calculate their estimated total GHG emissions and the percentage of improvements, as shown in Figure 17.

Table 12. Euro 5 fuel emission factors for diesel oil used in general transport [23].

Energy Content Factor (GJ/Kl)	Emission Factor Kg $CO_{2\text{-}e}$/GJ		
	CO_2	CH_4	N_20
38.6	69.9	0.06	0.5

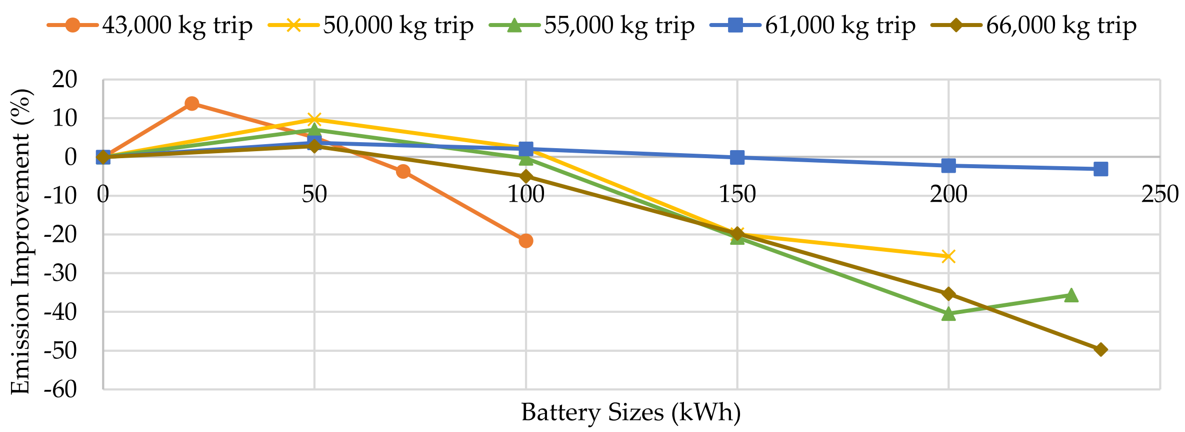

Figure 17. Total emission reduction in Victoria (0.96 kg $CO_{2\text{-}e}$/kWh).

From Figure 17, the charging of the TTRP hybrids or pure electric power train batteries of the power grid in Victoria will have a negative effect on reducing emissions in Australia. The method of electricity production is a challenge with power grid emission reductions. The amount of energy required to charge the batteries of the TTRP hybrids or pure electric power trains needed to come from renewable sources of energy, (e.g., charging emissions offset through use of solar panels) [49]. Furthermore, increasing the amount of electricity created from more renewable sources enabled the TTRP hybrids or pure electric power train to be feasible in reducing total emissions throughout the vehicle's life cycle. Using emission factors from neighboring states, as shown in Figures 18 and 19, provided a substantial improvement in reducing emissions and validating the option of operating with a 100 kWh battery. With emission factors falling to 0.35 kg $CO_{2\text{-}e}$/kWh, total emissions could be reduced, ranging from 6.5% to 55%, as depicted in Figure 19.

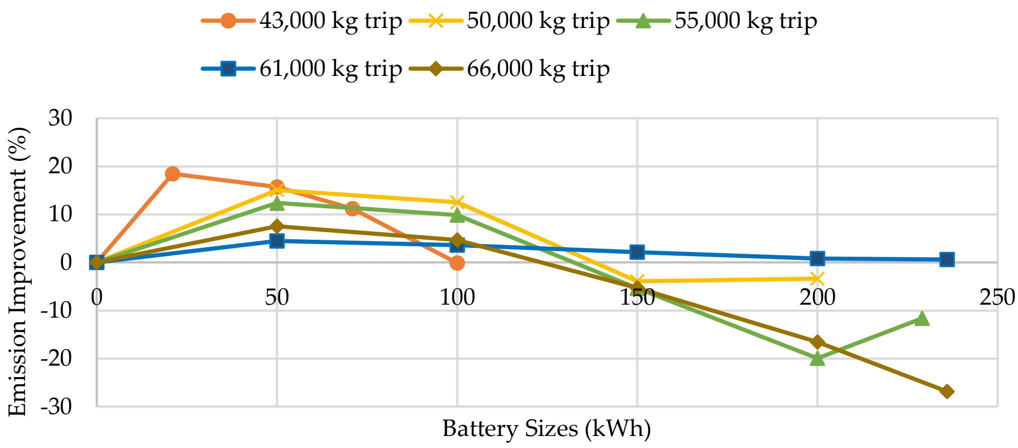

Figure 18. Total emission reduction in NSW (0.79 kg $CO_{2\text{-}e}$/kWh).

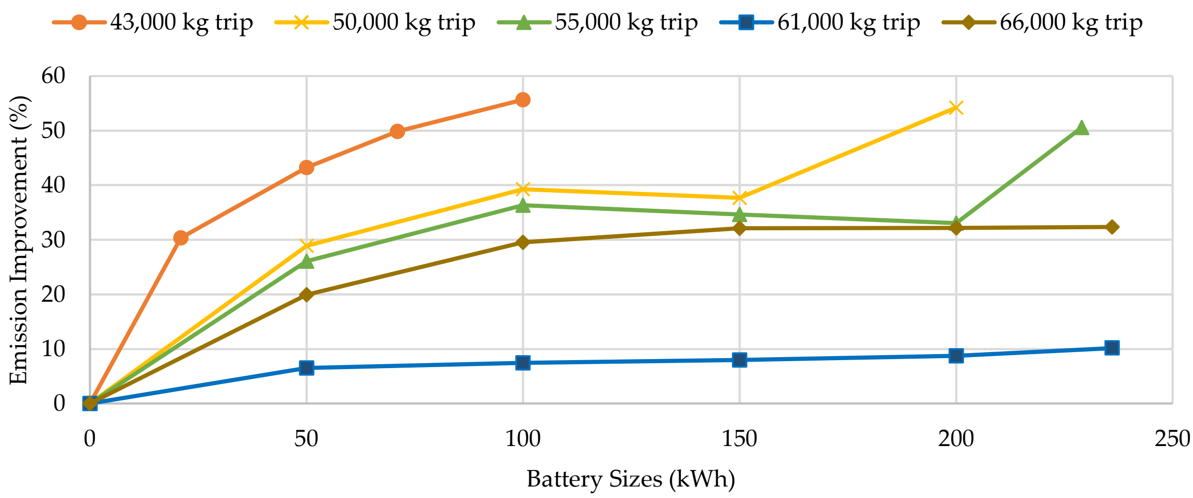

Figure 19. Total emission reduction in South Australia (0.35 kg $CO_{2\text{-}e}$/kWh).

6. Conclusions

This paper explored the feasibility of operating heavy multi-articulated vehicles with electric power trains within the Australian context to reduce carbon emissions. Real-world drive cycle data were obtained from the freight industry to model and simulate energy consumption of heavy multi-articulated freight vehicles. GCM up to 66,000 kg was simulated, with the largest battery weight reaching 2500 kg, leading to the heaviest GCM reaching 68,500 kg. A strong reduction in fuel consumption was found with the use of the TTRP hybrid configuration model, which, if implemented, could lead to cleaner air for freight operational areas. However, as battery sizes kept increasing, there was a turning point where reduction in total trip savings (fuel and electricity costs) was occurring. The additional weight of the battery did start to offset the efficiency gains of an electric power train, demonstrating that there will be an optimal TTRP hybrid power train for each different duty cycle. In addition, the carbon emissions created to charge the battery from the electricity plant can offset the total carbon emission reduction due to the large charging demands.

A battery size of 100 kWh was found to be optimal in peak reduction in operational costs (based on selected fuel and electric costs). However, the scenario of relying on the power grid to charge the batteries in Melbourne will cancel out the total carbon emissions' savings. Hence, decreasing the emissions factor for generating electricity down to 0.35 kg $CO_{2\text{-}e}$/kWh (as seen in South Australia) could allow charging off the grid in Melbourne and still gaining a strong reduction in total carbon emissions. Within the context of the Paris Agreement, the electrification of the RFIs will help meet reduction targets but it will also increase the need for methods to reduce emissions in the electricity sector. It is therefore recommended that Australia moves more quickly towards renewable energy sources to not only meet emissions targets but also to create a future that will permit the electrification of the RFIs and their benefits.

Author Contributions: Conceptualization, J.A. and A.K.; methodology, J.A.; software, J.A.; validation, J.A. and A.K.; formal analysis, J.A.; investigation, J.A.; resources, J.A.; data curation, J.A.; writing—original draft preparation, J.A.; writing—review and editing, J.A. and A.R.; visualization, J.A.; supervision, A.K.; project administration, A.K. and M.C.; funding acquisition, A.K. All authors have read and agreed to the published version of the manuscript.

Funding: This research was funded by Commonwealth, grant number 35600.

Acknowledgments: The authors thank Tiger Spider for its financial support of this work, along with other supporting industries that provided key empirical data.

Conflicts of Interest: The authors declare no conflict of interest.

References

1. Guandalini, G.; Campanari, S. Well-to-wheel driving cycle simulations for freight transportation: Battery and hydrogen fuel cell electric vehicles. In *2018 International Conference of Electrical and Electronic Technologies for Automotive*; IEEE: Piscataway, NJ, USA, 2018; pp. 1–6. [CrossRef]
2. Martins, P.P.P.; Boaventura, J.M.G.; Fischmann, A.A.; Costa, B.K.; Spers, R.G. Scenarios for the Brazilian road freight transport industry. *Foresight* **2012**, *14*, 207–224. [CrossRef]
3. Lena, L.; Emil, P.; Niklas, F. Type Vehicle Combinations—Hct Sweden 25.25 to 34 Meters. 2018. HVTT15. International Forum for Road Transport Technology. Available online: http://road-transport-technology.org//Proceedings/HVTT%2015//Larsson%20%20TYPE%20VEHICLE%20COMBINATIONS%20-%20HCT%20SWEDEN%2025.25%20TO%2034%20METERS.pdf (accessed on 1 July 2022).
4. Zhang, Y.; Thompson, R.G.; Bao, X.; Jiang, Y. Analyzing the Promoting Factors for Adopting Green Logistics Practices: A Case Study of Road Freight Industry in Nanjing, China. *Procedia Soc. Behav. Sci.* **2014**, *125*, 432–444. [CrossRef]
5. Lebedevas, S.; Dailydka, S.; Jastremskas, V.; Rapalis, P. Research of energy efficiency and reduction of environmental pollution in freight rail transportation. *Transport* **2017**, *32*, 291–301. [CrossRef]
6. Motasemi, F.; Afzal, M.T.; Salema, A.A.; Moghavvemi, M.; Shekarchian, M.; Zarifi, F.; Mohsin, R. Energy and exergy utilization efficiencies and emission performance of Canadian transportation sector, 1990–2035. *Energy* **2014**, *64*, 355–366. [CrossRef]
7. Çabukoglu, E.; Georges, G.; Küng, L.; Pareschi, G.; Boulouchos, K. Battery electric propulsion: An option for heavy-duty vehicles? Results from a Swiss case-study. *Transp. Res. Part C Emerg. Technol.* **2018**, *88*, 107–123. [CrossRef]
8. Australian Bureau of Statistics. 9208.0—Survey of Motor Vehicle Use, Australia, 12 Months Ended 30 June 2016. Available online: http://www.abs.gov.au/ausstats/abs@.nsf/mf/9208.0/ (accessed on 1 June 2018).
9. Dong, C.; Dong, X.; Jiang, Q.; Dong, K.; Liu, G. What is the probability of achieving the carbon dioxide emission targets of the Paris Agreement? Evidence from the top ten emitters. *Sci. Total Environ.* **2018**, *622–623*, 1294–1303. [CrossRef]
10. Bill, H.; Ursula, F.H.; Fabio, S.; Paola, P.; Jasmin, C.; Matt, B. The Finkel Review and Scientific Consistency with the Paris Agreement. Available online: https://climateanalytics.org/media/finkel_review_and_scientific_consistency_with_paris_agreement.pdf (accessed on 25 May 2018).
11. Ari, I.; Sari, R. Differentiation of developed and developing countries for the Paris Agreement. *Energy Strategy Rev.* **2017**, *18*, 175–182. [CrossRef]

12. Palander, T. The environmental emission efficiency of larger and heavier vehicles—A case study of road transportation in Finnish forest industry. *J. Clean. Prod.* **2017**, *155*, 57–62. [CrossRef]
13. Lammert, M.P.; Duran, A.; Diez, J.; Burton, K.; Nicholson, A. Effect of Platooning on Fuel Consumption of Class 8 Vehicles Over a Range of Speeds, Following Distances, and Mass. *SAE Int.* **2014**, *7*, 626–639. [CrossRef]
14. Lopes, M.; Serrano, L.; Ribeiro, I.; Cascão, P.; Pires, N.; Rafael, S.; Tarelho, L.A.D.C.; Monteiro, A.; Nunes, T.; Evtyugina, M.; et al. Emissions characterization from EURO 5 diesel/biodiesel passenger car operating under the new European driving cycle. *Atmos. Environ.* **2014**, *84*, 339–348. [CrossRef]
15. Dunn, S. Hydrogen futures: Toward a sustainable energy system. *Int. J. Hydrog. Energy* **2002**, *27*, 235–264. [CrossRef]
16. Edwards, P.P.; Kuznetsov, V.L.; David, W.I.F.; Brandon, N.P. Hydrogen and fuel cells: Towards a sustainable energy future. *Energy Policy* **2008**, *36*, 4356–4362. [CrossRef]
17. Holland, S.P.; Mansur, E.T.; Muller, N.Z.; Yates, A.J. Damages and Expected Deaths Due to Excess NOX Emissions from 2009 to 2015 Volkswagen Diesel Vehicles. *Environ. Sci. Technol.* **2016**, *50*, 1111–1117. [CrossRef] [PubMed]
18. Guan, B.; Zhan, R.; Lin, H.; Huang, Z. Review of the state-of-the-art of exhaust particulate filter technology in internal combustion engines. *J. Environ. Manag.* **2015**, *154*, 225–258. [CrossRef] [PubMed]
19. Onat, N.C.; Kucukvar, M.; Tatari, O. Conventional, hybrid, plug-in hybrid or electric vehicles? State-based comparative carbon and energy footprint analysis in the United States. *Appl. Energy* **2015**, *150*, 36–49. [CrossRef]
20. Bishop, J.D.K.; Martin, N.P.D.; Boies, A.M. Cost-effectiveness of alternative powertrains for reduced energy use and CO_2 emissions in passenger vehicles. *Appl. Energy* **2014**, *124*, 44–61. [CrossRef]
21. Sharma, R.; Manzie, C.; Bessede, M.; Crawford, R.H.; Brear, M.J. Conventional, hybrid and electric vehicles for Australian driving conditions. Part 2: Life cycle CO2-e emissions. *Transp. Res. Part C Emerg. Technol.* **2013**, *28*, 63–73. [CrossRef]
22. Zhou, B.; Wu, Y.; Zhou, B.; Wang, R.; Ke, W.; Zhang, S.; Hao, J. Real-world performance of battery electric buses and their life-cycle benefits with respect to energy consumption and carbon dioxide emissions. *Energy* **2016**, *96*, 603–613. [CrossRef]
23. Australian Government—Department of the Environment and Energy. National Greenhouse Accounts Factors. Available online: https://www.industry.gov.au/sites/default/files/August%202021/document/national-greenhouse-accounts-factors-2021.pdf (accessed on 22 August 2022).
24. Rosenbaum, A.; Hartley, S.; Holder, C. Analysis of diesel particulate matter health risk disparities in selected US harbor areas. *Am. J. Public Health* **2011**, *101*, S217–S223. [CrossRef]
25. EPA Victoria. Francis Street Monitoring Program—Finial Report. Available online: https://www.epa.vic.gov.au/our-work/publications/publication/2013/december/1546-1 (accessed on 25 May 2018).
26. Thompson, R.G.; Hassall, K. Implementing High Productivity Freight Vehicles in Urban Areas. *Procedia Soc. Behav. Sci.* **2014**, *151*, 318–332. [CrossRef]
27. National Heavy Vehicle Regulator, Australian Road Transport Suppliers Association. Performance Based Standards—Australia's PBS Fleet, A Joint Report by the NHVR and ARTSA. Available online: https://www.nhvr.gov.au/files/201805-0795-nhvr-artsa-pbs-report-may-2018.pdf (accessed on 27 June 2018).
28. Lee, D.-Y.; Thomas, V.M. Parametric modeling approach for economic and environmental life cycle assessment of medium-duty truck electrification. *J. Clean. Prod.* **2017**, *142*, 3300–3321. [CrossRef]
29. Ernst, C.-S.; Hackbarth, A.; Madlener, R.; Lunz, B.; Sauer, D.U.; Eckstein, L. Battery sizing for serial plug-in hybrid electric vehicles: A model-based economic analysis for Germany. *Energy Policy* **2011**, *39*, 5871–5882. [CrossRef]
30. Yabe, K.; Shinoda, Y.; Seki, T.; Tanaka, H.; Akisawa, A. Market penetration speed and effects on CO2 reduction of electric vehicles and plug-in hybrid electric vehicles in Japan. *Energy Policy* **2012**, *45*, 529–540. [CrossRef]
31. Liimatainen, H.; Pöllänen, M. Trends of energy efficiency in Finnish road freight transport 1995–2009 and forecast to 2016. *Energy Policy* **2010**, *38*, 7676–7686. [CrossRef]
32. Sen, B.; Ercan, T.; Tatari, O. Does a battery-electric truck make a difference?—Life cycle emissions, costs, and externality analysis of alternative fuel-powered Class 8 heavy-duty trucks in the United States. *J. Clean. Prod.* **2017**, *141*, 110–121. [CrossRef]
33. Hutchinson, T.; Burgess, S.; Herrmann, G. Current hybrid-electric powertrain architectures: Applying empirical design data to life cycle assessment and whole-life cost analysis. *Appl. Energy* **2014**, *119*, 314–329. [CrossRef]
34. Simmons, R.A.; Shaver, G.M.; Tyner, W.E.; Garimella, S.V. A benefit-cost assessment of new vehicle technologies and fuel economy in the U.S. market. *Appl. Energy* **2015**, *157*, 940–952. [CrossRef]
35. Zhang, Q.; Wu, L.; Yang, Z.; Zou, C.; Liu, X.; Zhang, K.; Mao, H. Characteristics of gaseous and particulate pollutants exhaust from logistics transportation vehicle on real-world conditions. *Transp. Res. Part D Transp. Environ.* **2016**, *43*, 40–48. [CrossRef]
36. Harald, N.; Bernd, B.; Joachim, R.; Wolfgang, N. *Automotive Transmissions Fundamentals, Selection, Design and Application*, 2nd ed.; Springer: Berlin/Heidelberg, Germany, 2011. [CrossRef]
37. Odhams, A.; Roebuck, R.; Lee, Y.; Hunt, S.; Cebon, D. Factors influencing the energy consumption of road freight transport. *Proc. Inst. Mech. Eng. Part C J. Mech. Eng. Sci.* **2010**, *224*, 1995–2010. [CrossRef]
38. Yuan, C.; Deng, Y.; Li, T.; Yang, F. Manufacturing energy analysis of lithium ion battery pack for electric vehicles. *CIRP Ann.* **2017**, *66*, 53–56. [CrossRef]
39. Saw, L.H.; Ye, Y.; Tay, A.A.O. Integration issues of lithium-ion battery into electric vehicles battery pack. *J. Clean. Prod.* **2016**, *113*, 1032–1045. [CrossRef]

40. Zhang, Y.; Wang, C.-Y.; Tang, X. Cycling degradation of an automotive LiFePO4 lithium-ion battery. *J. Power Sources* **2011**, *196*, 1513–1520. [CrossRef]
41. Song, Z.; Hofmann, H.; Li, J.; Han, X.; Ouyang, M. Optimization for a hybrid energy storage system in electric vehicles using dynamic programing approach. *Appl. Energy* **2015**, *139*, 151–162. [CrossRef]
42. Shabbir, W.; Evangelou, S.A. Real-time control strategy to maximize hybrid electric vehicle powertrain efficiency. *Appl. Energy* **2014**, *135*, 512–522. [CrossRef]
43. Song, Z.; Hofmann, H.; Li, J.; Hou, J.; Han, X.; Ouyang, M. Energy management strategies comparison for electric vehicles with hybrid energy storage system. *Appl. Energy* **2014**, *134*, 321–331. [CrossRef]
44. Zhang, S.; Xiong, R. Adaptive energy management of a plug-in hybrid electric vehicle based on driving pattern recognition and dynamic programming. *Appl. Energy* **2015**, *155*, 68–78. [CrossRef]
45. Li, L.; You, S.; Yang, C.; Yan, B.; Song, J.; Chen, Z. Driving-behavior-aware stochastic model predictive control for plug-in hybrid electric buses. *Appl. Energy* **2016**, *162*, 868–879. [CrossRef]
46. Yang, Y.L.; Hu, X.S.; Pei, H.X.; Peng, Z.Y. Comparison of power-split and parallel hybrid powertrain architectures with a single electric machine: Dynamic programming approach. *Appl. Energy* **2016**, *168*, 683–690. [CrossRef]
47. Zamboni, G.; André, M.; Roveda, A.; Capobianco, M. Experimental evaluation of Heavy Duty Vehicle speed patterns in urban and port areas and estimation of their fuel consumption and exhaust emissions. *Transp. Res. Part D Transp. Environ.* **2015**, *35*, 1–10. [CrossRef]
48. Thiruvengadam, A.; Besch, M.C.; Carder, D.K.; Oshinuga, A.; Gautam, M. Influence of Real-World Engine Load Conditions on Nanoparticle Emissions from a DPF and SCR Equipped Heavy-Duty Diesel Engine. *Environ. Sci. Technol.* **2012**, *46*, 1907–1913. [CrossRef]
49. Denholm, P.; Kuss, M.; Margolis, R.M. Co-benefits of large scale plug-in hybrid electric vehicle and solar PV deployment. *J. Power Sources* **2013**, *236*, 350–356. [CrossRef]